

Discrete Fractional Fourier Transform as a Fast Algorithm for Evaluating the Diffraction Pattern of Pulsed Radiation

Magdy Tawfik Hanna^{1,*}, Amr Mohamed Shaarawi², Nabila Philip Attalla Seif³ and Waleed Abd El Maguid Ahmed¹

¹ *Department of Engineering Mathematics and Physics, Faculty of Engineering, Fayoum University, Fayoum 63514, Egypt*

² *Department of Physics, The American University in Cairo, AUC Avenue, P.O. Box 74, New Cairo 11835, Egypt*

³ *Department of Engineering Mathematics and Physics, Faculty of Engineering, Cairo University, Giza 12613, Egypt*

*Corresponding author: mth00@fayoum.edu.eg

A new technique is proposed for computing the field radiated from a rectangular aperture. This technique, based on the Discrete FRactional Fourier Transform (DFRFT), avoids the complexities of computing the diffraction pattern by the direct evaluation of the Fresnel integral. The advocated approach provides a fast and accurate computational tool especially in the case of evaluating pulsed fields radiated through two-dimensional screens of complex amplitude. A detailed numerical study that demonstrates the efficacy of this approach is carried out. © 2010 Optical Society of America.

OCIS codes: 050.1940 (Diffraction), 260.0260 (Physical Optics), 320.5550 (Pulses).

1. Introduction

The method typically used to describe the propagation of radiation from an aperture to the Fourier domain is the Fresnel integral [1]. If it is not possible to evaluate the Fresnel integral analytically, it is customary to resort to numerical integration. However, the use of numerical integration for evaluating the Fresnel integral can be time consuming, especially when dealing with pulsed radiation from a two dimensional aperture.

Several alternative techniques have been proposed for the computation of the Fresnel integral. Examples of these include the algorithm proposed by Carcole *et al.* [2] which depends on approximating the highly oscillatory Fresnel integrals by means of three simpler integrals and providing analytical formulae for these three integrals by using geometrical properties of the diffraction pattern. D’Arcio *et al.* [3] developed a technique for calculating the near-field diffraction patterns by replacing the actual diffraction integrand by a variant of the Fresnel diffraction kernel. Subsequently, analytical solutions were derived for the alternative integral. These two techniques can deal with apertures of complicated shapes with acceptable accuracy. However, the accuracy depends to some extent on the approximations made to the Fresnel kernel.

Mas *et al.* [4] suggested a new technique for solving the Fresnel integral based on the similarity between the FRactional Fourier Transform (FRFT) and the Fresnel integral. Accordingly, the Fresnel integral is converted to the FRFT integral. The latter is evaluated by sampling it and then approximating it by a scaled version of the Discrete Fourier Transform (DFT). Subsequently, the DFT is calculated using either the single or double Fast Fourier Transform (FFT). The method is easy to implement but is affected by aliasing.

The present paper presents a new technique for evaluating the diffraction pattern based on the use of the Discrete FRactional Fourier Transform (DFRFT). The motivation behind this approach is that a Fresnel integral can be related to a scaled version of the continuous FRFT and the latter can be approximated by the DFRFT with high accuracy [5-6]. Consequently, the computation of the Fresnel integral will be reduced to the sampling of the amplitude distribution of the wave field at the source, and the premultiplication of the resulting excitation vector by DFRFT matrix to get samples of the output distribution at certain distance from the source. The core of this procedure is the technique for evaluating the DFRFT matrix.

In Section 2, the relation between the Fresnel integral and the FRFT is provided. The method of computing the DFRFT is explained in Section 3 and its utilization for approximating the FRFT is summarized in Section 4. In Section 5, the relation between the DFRFT and the Fresnel integral is extended to the two dimensional case. The numerical examples given in Section 6 testify to the effectiveness of the advocated approach in astonishingly reducing by several orders the computation time required for evaluating the Fresnel integral.

2. The relationship between the Fresnel integral and the FRFT

In this section, a different formulation is suggested to obtain the relationship between the Fresnel integral and the FRFT integral. This formulation is different from that previously used [e.g., cf. Ref. 4]. The a^{th} order continuous fractional Fourier transform has been defined by the integral [5]:

$$f_a(x) = \int_{-\infty}^{\infty} K_a(x, x') f(x') dx' \quad (1-a)$$

where

$$K_a(x, x') = \begin{cases} \sqrt{\frac{1 - i \cot(\alpha)}{2\pi}} \exp\left[i 0.5 (x^2 \cot(\alpha) - 2xx' \csc(\alpha) + x'^2 \cot(\alpha))\right] & \text{if } \alpha \text{ isn't a multiple of } \pi \\ \delta(x - x') & \text{if } \alpha \text{ is a multiple of } 2\pi \\ \delta(x + x') & \text{if } \alpha + \pi \text{ is a multiple of } 2\pi \end{cases} \quad (1-b)$$

and $\alpha = \pi a/2$ is the angle of rotation. More specifically $f_a(x)$ is a representation of the signal $f(x)$ along an axis making an angle α with the time axis in the time-frequency plane.

Consider radiation of wavelength λ illuminating a planar screen with complex amplitude transmittance $t(x)$. The diffraction field of such radiation produces a complex amplitude distribution of light $\hat{A}(x)$ in a plane at distance d from the screen given by the Fresnel integral [6]:

$$\hat{A}(x) = \int_{-\infty}^{\infty} h_{space}(x, x', k) t(x') dx' \quad (2-a)$$

where $h_{space}(x, x', k)$ is the kernel of the Fresnel integral defined by:

$$h_{space}(x, x', k) = \exp\left(i \frac{2\pi d}{\lambda}\right) \sqrt{\frac{1}{i\lambda d}} \exp\left[i \frac{\pi}{\lambda d} (x - x')^2\right] \quad (2-b)$$

where $k = 1/\lambda$ is the wavenumber.

In preparation for expressing the Fresnel integral in terms of the FRFT, one starts by rewriting (1-a) as:

$$f_a(x) = \frac{1}{L} \int_{-\infty}^{\infty} K_a\left(x, \frac{x'}{L}\right) f\left(\frac{x'}{L}\right) dx' \quad (3)$$

where L is half the width of the aperture.

Based on (1-b), the main part of the exponent of the complex exponential term appearing in

$K_a\left(x, \frac{x'}{L}\right)$ can be manipulated as follows:

$$\begin{aligned}
& 0.5 x^2 \cot(\alpha) - x \left(\frac{x'}{L}\right) \csc(\alpha) + 0.5 \left(\frac{x'}{L}\right)^2 \cot(\alpha) \\
&= \frac{0.5 \cot(\alpha)}{L^2} [x'^2 - 2Lxx' \sec(\alpha) + L^2 x^2] \\
&= \frac{0.5 \cot(\alpha)}{L^2} \{ [x' - Lx \sec(\alpha)]^2 + L^2 [1 - \sec^2(\alpha)] x^2 \} \\
&= -0.5 \tan(\alpha) x^2 + \frac{0.5 \cot(\alpha)}{L^2} [x' - Lx \sec(\alpha)]^2 .
\end{aligned} \tag{4}$$

Consequently $f_a(x)$ in Eq. (3) can be expressed as:

$$f_a(x) = \frac{1}{L} \sqrt{\frac{1 - i \cot(\alpha)}{2\pi}} \exp(-i0.5 \tan(\alpha) x^2) \int_{-\infty}^{\infty} \exp\left(i \frac{0.5 \cot(\alpha)}{L^2} [x' - Lx \sec(\alpha)]^2\right) f\left(\frac{x'}{L}\right) dx' . \tag{5}$$

In order for the above integral to resemble in its appearance that of (2), replace x by $\frac{x}{L} \cos(\alpha)$

in both sides of the above equation to get:

$$f_a\left(\frac{x}{L} \cos(\alpha)\right) = \frac{1}{L} \sqrt{\frac{1 - i \cot(\alpha)}{2\pi}} \exp\left(-i0.25 \sin(2\alpha) \left(\frac{x}{L}\right)^2\right) \int_{-\infty}^{\infty} \exp\left(i \frac{0.5 \cot(\alpha)}{L^2} [x' - x]^2\right) f\left(\frac{x'}{L}\right) dx' . \tag{6}$$

By comparing the integral appearing in the above equation with that in (2), one is naturally led to define a scaled version $t^s(x)$ of $t(x)$ as follows:

$$t^s(x) = t(Lx) . \tag{7}$$

Consequently (2) can be expressed as:

$$\hat{A}(x) = \exp\left(i \frac{2\pi d}{\lambda}\right) \sqrt{\frac{1}{i\lambda d}} \cdot \int_{-\infty}^{\infty} \exp\left[i \frac{\pi}{\lambda d} (x - x')^2\right] t^s\left(\frac{x'}{L}\right) dx' . \tag{8}$$

Upon comparing (6) and (8) one concludes that in order to express $\hat{A}(x)$ in terms of the FRFT of $t^s(x)$, the angle α should be selected such that $0.5(\cot(\alpha)/L^2) = \pi/\lambda d$ or

$$\alpha = \tan^{-1}\left(\frac{\lambda d}{2\pi L^2}\right). \quad (9)$$

Consequently

$$\begin{aligned} \sin(2\alpha) &= 2\sin(\alpha)\cos(\alpha) \\ &= 2\frac{(\lambda d)(2\pi L^2)}{(2\pi L^2)^2 + (\lambda d)^2}. \end{aligned} \quad (10)$$

Expressing (8) in the light of (6) where α is given by (9), one obtains:

$$\hat{A}(x) = \sqrt{\frac{1}{i\lambda d}} \exp\left(i\frac{2\pi d}{\lambda}\right) L \sqrt{\frac{2\pi}{1-i\cot(\alpha)}} \exp\left[i0.25\sin(2\alpha)\left(\frac{x}{L}\right)^2\right] t_a^s\left(\frac{x}{L}\cos(\alpha)\right). \quad (11)$$

where $t_a^s(x)$ is the FRFT of $t^s(x)$. Using (9), the above equation can be expressed in terms of α solely as:

$$\hat{A}(x) = \sqrt{\frac{1}{1+i\tan(\alpha)}} \exp\left(i\left(\frac{2\pi L}{\lambda}\right)^2 \tan(\alpha)\right) \exp\left[i0.25\sin(2\alpha)\left(\frac{x}{L}\right)^2\right] t_a^s\left(\frac{x}{L}\cos(\alpha)\right). \quad (12)$$

Alternatively, using (9) and (10), $\hat{A}(x)$ can be expressed in terms of d solely as:

$$\hat{A}(x) = \sqrt{\frac{1}{1+i\frac{\lambda d}{2\pi L^2}}} \exp\left(i\frac{2\pi d}{\lambda}\right) \exp\left[i\frac{\pi\lambda d}{(\lambda d)^2 + (2\pi L^2)^2} x^2\right] t_a^s\left(\frac{2\pi L}{\sqrt{(\lambda d)^2 + (2\pi L^2)^2}} x\right). \quad (13)$$

By defining a new variable u as $u = \frac{x}{L}\cos(\alpha)$, Eq. (12) can be expressed as:

$$\tilde{A}(u) \equiv \hat{A}(Lu\sec(\alpha)) = \sqrt{\frac{1}{1+i\tan(\alpha)}} \exp\left(i\left(\frac{2\pi L}{\lambda}\right)^2 \tan(\alpha)\right) \exp\left[i0.5\tan(\alpha)u^2\right] t_a^s(u). \quad (14)$$

Equation (9) implies that the angle α is directly determined by the distance d between the plane where the distribution of light $\hat{A}(x)$ is sought and the illuminated planar screen. An inspection of (9) shows that $\alpha \rightarrow \pi/2$ and consequently $a \rightarrow 1$ as $d \rightarrow \infty$. It follows from Eq. (13) that

$$\lim_{d \rightarrow \infty} \hat{A}(x) = 0 .$$

Practically for $a > 0.8$ one is essentially calculating the field in the Fraunhofer region where the diffraction pattern reduces to the Fourier transform of the screen. Another special case arises in the Rayleigh limit where $a = 1/2$ and consequently $\alpha = \pi/4$. In this case (9) implies that $d = 2\pi L^2/\lambda$, the Rayleigh diffraction limit, and (12) simplifies to:

$$\hat{A}(x) \Big|_{d=\frac{2\pi L^2}{\lambda}} = \sqrt{\frac{1}{1+i}} \exp\left(i\left(\frac{2\pi L}{\lambda}\right)^2\right) \exp\left[i0.25\left(\frac{x}{L}\right)^2\right] t_{0.5}^s\left(\frac{1}{\sqrt{2}}\frac{x}{L}\right) . \quad (15)$$

3. The Discrete Fractional Fourier Transform

In the recent years, methods for defining and evaluating the DFRFT have been developed as an alternative to the numerical evaluation of the integral appearing in the definition of the FRFT given by Eq. (1). The advocated DFRFT techniques may be regarded as a generalization of the DFT. Along such veins, most of the available techniques start by the analysis equation of the DFT, viz.,

$$\mathbf{X}[p] = \frac{1}{\sqrt{N}} \sum_{q=0}^{N-1} W_N^{pq} x[q] ; p = 0,1,2,\dots,N-1 \quad (16.a)$$

where

$$W_N = \exp\left[-i \frac{2\pi}{N}\right]. \quad (16.b)$$

This can be written in matrix form as $\mathbf{X} = \mathbf{F}\mathbf{x}$, where the DFT matrix \mathbf{F} is defined by:

$$\mathbf{F} = [f_{pq}] \text{ and } f_{pq} = \frac{1}{\sqrt{N}} W_N^{(p-1)(q-1)}, \quad p, q = 1, 2, \dots, N.$$

The eigen-decomposition of the DFT matrix \mathbf{F} is $\mathbf{F} = \mathbf{M}\mathbf{D}\mathbf{M}^{-1}$, where \mathbf{M} is a modal matrix that has the eigenvectors of \mathbf{F} as its columns and \mathbf{D} is a diagonal matrix whose diagonal elements are the eigenvalues of \mathbf{F} . Inspired by this formulation, the DFRFT of the fractional order a can be defined by:

$$\mathbf{X} = \mathbf{F}^a \mathbf{x} \quad (17.a)$$

where:

$$\mathbf{F}^a \equiv \mathbf{M}\mathbf{D}^a\mathbf{M}^{-1}. \quad (17.b)$$

This means that the fractional power of matrix \mathbf{F} is calculated from its eigendecomposition and the fractional powers of its eigenvalues. The definition of the DFRFT should satisfy the following conditions [5]:

1. Unitarity.
2. Index additivity.
3. Reduction to the DFT matrix for unity order ($a = 1$).
4. Achieving a good approximation of the FRFT.

The first two conditions are satisfied by selecting orthonormal eigenvectors for the matrix \mathbf{F} . The third condition is directly satisfied by virtue of Eq. (17.b). The fourth requirement will be satisfied by choosing eigenvectors whose elements resemble the Hermite-Gaussian functions, since they are the eigenfunctions of both the continuous-time Fourier transform (CTFT) and the FRFT.

In their pioneering work, McClellan and Parks [7] arrived at the multiplicities of the eigenvalues of matrix \mathbf{F} . Santhanam and McClellan were the first to try to develop a definition for the DFRFT through the eigendecomposition of matrix \mathbf{F} [8]. Unfortunately this definition was later shown – by Pei et al. [5,9] – not to be a fully-fledged one since it is inherently the sum of four terms; namely the time-domain signal and its DFT together with their circularly reflected versions. Dickinson and Steiglitz [10] arrived at a real symmetric nearly tridiagonal matrix \mathbf{S} which commutes with matrix \mathbf{F} and proved that the maximum algebraic multiplicity of any of its eigenvalues can be two; which occurs only when the order N of the matrix is a multiple of 4. Although a common set of eigenvectors of \mathbf{S} and \mathbf{F} always exists, the case of a double eigenvalue of \mathbf{S} requires special attention since a set of two corresponding eigenvectors of \mathbf{S} – obtained by a general eigenanalysis software package – will generally neither be eigenvectors of \mathbf{F} nor even be orthogonal. Candan, Kutay and Ozaktas [11] applied a similarity transformation defined in terms of a unitary matrix \mathbf{P} to matrix \mathbf{S} and argued that \mathbf{PSP}^{-1} is a 2 x 2 block diagonal matrix and that the two diagonal blocks are unreduced tridiagonal matrices. They showed that the eigenvectors of \mathbf{S} are Hermite-Gaussian-like. Pursuing it further, Pei et al. viewed the orthonormal eigenvectors of \mathbf{S} as only *initial* eigenvectors of \mathbf{F} and generated *final* ones which better approximate the Hermite-Gaussian functions by using either the orthogonal procrustes algorithm (OPA) or the Gram-Schmidt algorithm (GSA) [5]. Hanna, Seif and Ahmed proved that those *final* eigenvectors are invariant under the change of the *initial* ones [12]. Moreover they developed a methodology for the generation of the *final* superior eigenvectors - without computing the *initial* ones as a prerequisite - based on the direct utilization of the orthogonal projection matrices of the DFT matrix on its eigenspaces [13].

It is worth mentioning that matrix \mathbf{S} used in [10,11,5] is based on a second order approximation to the second derivative appearing in the differential equation generating Hermite-Gaussian functions. Recently Candan [14] used higher order approximations to the second derivative and the resulting difference equation is expressed in terms of a circulant matrix \mathbf{M} of order N . The highest approximation order ($2k$) should satisfy $2k + 1 \leq N$. The generating matrix \mathbf{M} is used in obtaining a matrix which commutes with the DFT matrix \mathbf{F} and whose eigenvectors better approximate samples of the Hermite-Gaussian functions than those of matrix \mathbf{S} used in [10,11,5]. More recently Pei, Hsue and Ding [15] removed the order upper bound restriction and constructed arbitrary order DFT-commuting matrices whose Hermite-Gaussian-like eigenvectors outperform those of [14]. Serbes and Durak-Ata [16] obtained an exact closed-form expression for the infinite order approximation to the second derivative in terms of inverse trigonometric functions.

In the present paper, one first generates the eigenvectors of matrix \mathbf{S} of [10] using the procedure advocated in [11]. Taking them as *initial* eigenvectors of the DFT matrix \mathbf{F} , one next generates the *final* superior ones using the Gram-Schmidt algorithm (GSA) contributed in [5]. Since it was proved that the *final* eigenvectors of \mathbf{F} are invariant under the change of the *initial* ones [12], the approach of the present paper outperforms those of [14-16]. As a final remark the digital method for computing the continuous FRFT – without using the notion of the DFRFT – contributed by Ozaktas et al. [17] has been avoided since it does not preserve the index additivity property.

4. Relationship between DFRFT and FRFT

Consider the continuous signal $f(t)$ defined on the interval $-L \leq t \leq L$, the procedure adopted for calculating the FRFT of $f(t)$ with an angular parameter α using the DFRFT of the preceding section is as follows:

1. Sample the function $f(t)$ with sampling interval T_s given by

$$T_s = \frac{2L}{N_s} \quad (18)$$

where N_s is the number of sampling points.

2. Zero pad to the right and left of the sampled function $f(nT_s)$ such that the total number of samples will be N .
3. Construct vector \mathbf{x} whose elements are the sequence $x[q]$ defined by:

$$x[q] = \begin{cases} f(qT_s) & \text{for } 0 \leq q \leq \frac{N}{2} - 1 \\ f((q-N)T_s) & \text{for } \frac{N}{2} \leq q \leq N-1 \end{cases} \quad \text{for even } N, \quad (19-a)$$

$$x[q] = \begin{cases} f(qT_s) & \text{for } 0 \leq q \leq \frac{N-1}{2} \\ f((q-N)T_s) & \text{for } \frac{N+1}{2} \leq q \leq N-1 \end{cases} \quad \text{for odd } N. \quad (19-b)$$

4. Compute the modified angle β :

$$\beta = \tan^{-1} \left[\left(\frac{2\pi}{NT_s^2} \right) \tan \alpha \right]. \quad (20)$$

5. Compute the vector:

$$\mathbf{X}_\beta = \mathbf{F}^{\frac{2}{\pi}\beta} \mathbf{x}. \quad (21)$$

The elements of vector \mathbf{X}_β are the DFRFT sequence $X_\beta[p]$, $p = 0, 1, \dots, N-1$.

6. Calculate the spacing Δ_α between the samples of the FRFT using the formula [5]:

$$\Delta_\alpha = \sqrt{T_s^2 \cos^2(\alpha) + \frac{4\pi^2}{N^2 T_s^2} \sin^2(\alpha)}. \quad (22)$$

7. Compute the DFRFT with an angle of rotation α using the elementwise multiplication:

$$X_\alpha[p] = P_D[p] X_\beta[p], \quad p = 0, 1, \dots, N-1. \quad (23)$$

where $P_D[p]$ is the postphase compensation factor given by [5]:

$$P_D[p] = \sqrt{\frac{N}{2\pi}} T_s \sqrt{\frac{1 - i \cot(\alpha)}{1 - i \frac{N}{2\pi} T_s^2 \cot(\alpha)}} \exp\left(i \frac{p^2 \Delta_\alpha^2}{2} \left(1 - \frac{\cos^2(\beta)}{\cos^2(\alpha)}\right) \cot \alpha\right). \quad (24)$$

Having obtained the DFRFT X_α , one can directly get the samples of the FRFT using the formula:

$$f_\alpha(p\Delta_\alpha) = \begin{cases} X_\alpha[p] & \text{for } 0 \leq p \leq \frac{N}{2} - 1 \\ X_\alpha[p + N] & \text{for } -\frac{N}{2} \leq p \leq -1 \end{cases} \quad \text{for N even,} \quad (25-a)$$

$$f_\alpha(p\Delta_\alpha) = \begin{cases} X_\alpha[p] & \text{for } 0 \leq p \leq \frac{N-1}{2} \\ X_\alpha[p + N] & \text{for } -\frac{N-1}{2} \leq p \leq -1 \end{cases} \quad \text{for N odd.} \quad (25-b)$$

One should note that:

- The zero padding in step 2 is required in order for the N samples to reflect the true nature of the continuous-time signal $f(t)$.
- Step 3 is required since the support of the signal $f(t)$ can include part of the negative time axis. Employing the DFT to transform the sequence $x[n]$ to the sequence $X[k]$ implies

that the underlying mathematical framework is periodic [18], i.e. $x[n]$ is one period of a periodic signal with period N and the same holds for $X[k]$. The same notion should hold for the DFRFT.

- Steps 4, 6 and 7 were suggested by Pei *et. al.* [5] because the sampling period T_s in (18) is generally not equal to $\sqrt{2\pi/N}$. In the very special case of $T_s = \sqrt{2\pi/N}$ one has the simplification: $\beta = \alpha$, $\Delta_\alpha = T_s$ and $P_D = 1$.

5. Diffraction from a rectangular aperture

The relationship between the FRFT and the Fresnel integral that has been elaborated upon in section 2 can be generalized to the two-dimensional case, under the assumption that the amplitude of the optical signal is separable, viz.,

$$\phi(x, y) = f(x)g(y). \quad (26)$$

The FRFT of the two-dimensional function $\phi(x, y)$ is given by:

$$\phi_a(x, y) = \int_{-\infty}^{\infty} \int_{-\infty}^{\infty} h_a(x, x'; y, y'; k) \phi(x', y') dx' dy' \quad (27)$$

where

$$h_a(x, x'; y, y'; k) = K_a(x, x')K_a(y, y') \quad (28)$$

and K_a is defined by (1-b). It follows that

$$\phi_a(x, y) = f_a(x)g_a(y). \quad (29)$$

The DFRFT that approximates the FRFT of $\phi(x, y)$ is the product of the DFRFTs of the sampled version of both $f(x)$ and $g(y)$.

The diffraction from a planar screen with complex amplitude transmittance $t(x, y)$ produces a complex amplitude distribution $\hat{A}(x, y)$ of light in a diffraction plane at distance d from the illuminated screen according to the Fresnel integral [Ref. 6, p. 232, Eqs. (7.43) and (7.44)]:

$$\hat{A}(x, y) = \int_{-\infty-\infty}^{\infty} \int_{-\infty-\infty}^{\infty} h_{space}(x, x'; y, y'; k) t(x', y') dx' dy' \quad (30)$$

where

$$h_{space}(x, x'; y, y'; k) = \exp(i2\pi d/\lambda) \frac{1}{i\lambda d} \exp\left(\frac{i\pi[(x-x')^2 + (y-y')^2]}{\lambda d}\right). \quad (31)$$

For a separable two-dimensional amplitude transmittance

$$t(x, y) = t^{(1)}(x) t^{(2)}(y) \quad (32)$$

the two-dimensional amplitude distribution of light in a diffraction plane at distance d is obtained using (12) as:

$$\hat{A}(x, y) = A_0 \exp\left\{i0.25 \left[\left(\frac{x}{L_1}\right)^2 \sin(2\alpha_1) + \left(\frac{y}{L_2}\right)^2 \sin(2\alpha_2) \right]\right\} t_{a_1}^{(1)s} \left(\frac{x}{L_1} \cos(\alpha_1)\right) t_{a_2}^{(2)s} \left(\frac{y}{L_2} \cos(\alpha_2)\right) \quad (33)$$

where:

$$A_0 = \frac{1}{\sqrt{1+i \tan(\alpha_1)}} \frac{1}{\sqrt{1+i \tan(\alpha_2)}} \exp\left(i \frac{2\pi d}{\lambda}\right), \quad (34)$$

$$\alpha_1 = \tan^{-1}\left(\frac{\lambda d}{2\pi L_1^2}\right); \quad \alpha_2 = \tan^{-1}\left(\frac{\lambda d}{2\pi L_2^2}\right). \quad (35)$$

In the above equations L_1 and L_2 are half the width of the aperture in the x and y directions respectively. Letting $u = \frac{x}{L_1} \cos(\alpha_1)$ and $v = \frac{y}{L_2} \cos(\alpha_2)$, Eq. (33) leads to:

$$\tilde{A}(u, v) \equiv \hat{A}(L_1 u \sec(\alpha_1), L_2 v \sec(\alpha_2)) = A_0 \exp\{i0.5[u^2 \tan(\alpha_1) + v^2 \tan(\alpha_2)]\} t_{a_1}^{(1)s}(u) t_{a_2}^{(2)s}(v). \quad (36)$$

One should notice that if the rectangular aperture is replaced by a square one, then $L_1 = L_2 = L$; $\alpha_1 = \alpha_2 = \alpha$ and (33) reduces to:

$$\hat{A}(x, y) = \frac{1}{1 + i \tan(\alpha)} \exp\left(i \frac{2\pi d}{\lambda}\right) \exp\left[\frac{i \sin(2\alpha)}{4L^2}(x^2 + y^2)\right] t_a^{(1)s}\left(\frac{x}{L} \cos(\alpha)\right) t_a^{(2)s}\left(\frac{y}{L} \cos(\alpha)\right). \quad (37)$$

6. Numerical Examples

In preceding sections, it has been shown that the FRFT can solve the Fresnel integral which is used to determine the diffraction pattern. It has also been alluded to the fact that the DFRFT can be used to evaluate the FRFT and consequently to determine the diffraction pattern. Consequently the Fresnel integral can be evaluated by replacing the integration operation by just matrix multiplication. The effectiveness of the DFRFT is demonstrated by considering several numerical simulations of the diffraction from rectangular apertures. The two cases dealing with continuous wave and pulsed illuminations are considered.

A) Continuous Wave Illumination

Consider the case of a long rectangular slit illuminated by a uniform radiation distribution having wavelength λ . Assume that the width of the aperture in the x -direction is 4 units (i.e. $2L = 4$). All lengths are given in terms of an arbitrary unit which would depend on the width of the aperture $2L$. The length of the slit in the y -direction is much longer than the wavelength such that diffraction effects along this direction are negligible and the one-dimensional Fresnel integral can be used to determine the radiated field. Furthermore, choose the light wavelength λ equal to $0.025L$ with light amplitude:

$$v(x) \equiv \text{rect}\left(\frac{x}{2L}\right) = \begin{cases} 1 & -L < x < L \\ 0.5 & x = \pm L \\ 0 & \text{otherwise} \end{cases} . \quad (38)$$

The plots in Fig. (1) show the real and imaginary parts of the diffraction pattern calculated at distance $d = 2.5L$. The solid line plots represent the Fresnel Integral evaluated using the **Recursive Adaptive Lobatto Quadrature (RALQ) method which approximates the definite integral to within an error of 10^{-6}** [19]. The dots on the same plots are obtained using the DFRFT with $N = 500$. The two plots demonstrate that the radiation patterns calculated using the **RALQ evaluation method** of the Fresnel integral and the DFRFT are quite close to each other. To illustrate the efficacy of the DFRFT algorithm, the same calculation is repeated for $N = 70$. The resulting values are plotted in Fig. (2) where one notices the slight degradation in the degree of match due to decreasing N .

The same calculations are repeated at a closer distance to the aperture, namely $d = L$. And for a shorter wavelength. The effectiveness of the DFRFT approach for evaluating the Fresnel integral as compared to **RALQ method** will be studied by recording the computation time. While the width of the aperture is kept the same, the wavelength is chosen equal to $0.001L$. The solid curve in Fig. (3) shows the real and imaginary parts calculated using **RALQ method** for evaluating the Fresnel integral, while the dots represent the values calculated using DFRFT with $N = 500$. In Fig. (4), the same plots are repeated but with the DFRFT calculated using $N = 70$. One should note that for shorter wavelength the error in DFRFT calculation is relatively high around the sharp transition edges. In Table (1), the computation time of the DFRFT and the **RALQ method** are compared. The entries in the table are the execution times for runs carried out on **Dell latitude E6510 Intel® core™ i5 CPU M520 @ 2.40GHz 1.17 GHz, 1.99 GB of RAM,**

232.8 GB of HDD computer laptop. The saving in the execution time when using the DFRFT approach is unequivocal.

The following two examples demonstrate the effectiveness of using the DFRFT for computing the diffraction pattern for the radiation from a two-dimensional rectangular aperture. The width parameters are $L_1 = L_2 = L = 2$, $v(x,y) = v(x)v(y) = \text{rect}\left(\frac{x}{4}\right)\text{rect}\left(\frac{y}{4}\right)$, and the wavelength $\lambda = 0.025L$. The real part of the radiated field at $d = 0.25L$ is displayed in Fig. (5). The surface plot in Fig. (5-a) is evaluated by using the **RALQ method**, while Fig. (5-b) is calculated using DFRFT with $N = 70$. The execution times of the **RALQ method** and the DFRFT are compared in Table (2). One should notice the advantage of the DFRFT as far as the computation time is concerned. The effectiveness of the DFRFT method becomes clearer when one considers the case of a shorter wavelength radiation. Fig. (6) illustrates the surface plots evaluated using the **RALQ** and DFRFT methods for $\lambda = 0.00025L$. The other conditions are maintained as in Fig. (5).

B) Pulsed Illumination

Consider an aperture illuminated by a wavefield whose spectrum is given by [20]:

$$\hat{f}(x, k) = \text{rect}\left(\frac{x}{2L}\right) k^\mu \exp(-2\pi k c T) \quad (39)$$

where $k = 1/\lambda$ is the wave number, T is the pulse duration, μ is a parameter that determines the bandwidth and the peak of the spectrum of the pulse, and c is the velocity of light in vacuum.

The above equation can be expressed as:

$$\hat{f}(x, k) = v(x) b(k) \quad (40)$$

where $v(x)$ is given by Eq. (38) and $b(k)$ is the amplitude of the spectrum at the aperture given by:

$$b(k) = k^\mu \exp(-2\pi k c T) . \quad (41)$$

The spectrum of the radiated field at distance d from the aperture is:

$$\hat{G}(x, k) = \int_{x'=-\infty}^{\infty} h_{space}(x, x', k) \hat{f}(x', k) dx' . \quad (42)$$

Upon substituting (40) in (42), one obtains:

$$\hat{G}(x, k) = b(k) \int_{x'=-\infty}^{\infty} h_{space}(x, x', k) v(x') dx' . \quad (43)$$

Applying the result (12), the above equation can be expressed as:

$$\hat{G}(x, k) = b(k) \frac{1}{\sqrt{1 + i \tan(\alpha)}} \exp[i(2\pi L k)^2 \tan(\alpha)] \exp\left[i0.25 \sin(2\alpha) \left(\frac{x}{L}\right)^2\right] v_a^s\left(\frac{x}{L} \cos(\alpha)\right) \quad (44)$$

where $v^s(x) = v(Lx)$ and $\alpha = \tan^{-1}\left(\frac{d}{2\pi L^2 k}\right)$. By taking the inverse Fourier transform, one

obtains the radiated field as:

$$G(x, t) = \int_{k=0}^{\infty} \exp(-i2\pi k c t) \hat{G}(x, k) dk . \quad (45)$$

Upon using Eqs. (44) and (41), one obtains:

$$G(x, t) = \int_{k=0}^{\infty} \exp(-i2\pi k c t) k^\mu \exp(-2\pi k c T) \frac{1}{\sqrt{1 + i \tan(\alpha)}} \exp\left[i(2\pi L k)^2 \tan(\alpha)\right] \exp\left[i0.25 \sin(2\alpha) \left(\frac{x}{L}\right)^2\right] v_a^s\left(\frac{x}{L} \cos(\alpha)\right) dk \quad (46)$$

It should be mentioned that without the notion of the FRFT, the above radiated pulse can be obtained by substituting (43), (41), (38), and (2-b) in Eq. (45) to get

$$G(x, t) = \int_{k=0}^{\infty} \exp(-i2\pi kct) k^{\mu} \exp(-2\pi k c T) \exp(i2\pi dk) \sqrt{\frac{k}{id}} \int_{x'=-L}^{+L} \exp\left[i \frac{\pi k}{d} (x-x')^2\right] dx' dk. \quad (47)$$

Let the width of the aperture be $2L = 2$ and the parameter values be $\mu = 10$ and $cT = 0.6$. The corresponding amplitude of the spectrum $b(k)$ of (41) is displayed in Fig. (7) which shows that all significant spectral components fall in the range $0 \leq k \leq 7$. The radiated pulse $G(x, t)$ at distance $d = 0.5L$ is computed using both the **RALQ** rule to evaluate the double integral in (47) and the DFRFT to approximate the FRFT in preparation for the numerical evaluation of the single integral appearing in (46) (where k varies from 0.1 to 7). The surface plots of the wavefield are displayed in Fig. (8), where the plotting grid has increments $\Delta x = 0.1$ and $\Delta t = 0.01/c$ second (where ct takes values from 0.1 to 1.2). The computation times of both methods are shown in Table (3) which demonstrates the substantial saving achieved by the DFRFT method. The profiles of the radiated pulse evaluated at $x = L$ as computed by the two methods are shown in Fig. (9) which testifies to the sufficient accuracy of the DFRFT method.

7. Concluding Remarks

The Fresnel integral has been expressed in terms of the continuous FRactional Fourier Transform (FRFT) and consequently it has been evaluated using the Discrete FRactional Fourier Transform (DFRFT) as a fast and accurate alternative to the numerical integration method. The proposed method has been successfully applied for finding the diffraction pattern of an illuminated rectangular screen in both the one- dimensional and two-dimensional cases. The simulation results exhibit a tremendous improvement in the computation time of the DFRFT approach as compared to the **RALQ** rule numerical integration technique.

Although the technique described in this paper is limited to rectangular optical elements and apertures, it is of interest to extend this approach to more general shapes especially circular optical components. For circular elements, the evaluation of the diffraction field can be achieved by making use of the fractional Hankel transform (FRHT). There have been several attempts to evaluate FRHT directly or through relating it to the FRFT [21-23]. To achieve this goal an approach similar to the one used in this paper may be used. An analogous discrete fractional Hankel transform (DFRHT) approach will be based on the construction of the fractional transformation matrix through the calculation of its eigendecomposition and the fractional powers of the eigenvalues. In the case of circular optical element, the eigenvalues are represented either by the two-variable Hermite polynomials or the Laguerre–Gauss modes [21,22]. Generalization to 2-D optical elements of arbitrary shape may be done by using techniques similar to the one described in [24].

ACKNOWLEDGEMENT

The First author acknowledges the financial support of the Science and Technology Development Fund (STDF), Egypt, Grant No. 2091.

REFERENCES

1. J. W. Goodman, *Introduction to Fourier Optics*, second edition, New York: McGraw-Hill, 1996.
2. E. Carcole, S. Bosch and J. Campos, "Analytical and numerical approximations in Fresnel diffraction procedures based on the geometry of the Cornu spiral," *Journal of Modern Optics*, 40, No. 6, pp. 1091-1106, January 1993.
3. L. A. D'Arcio, J. M. Braat, and H. J. Frankena, "Numerical evaluation of diffraction integrals for apertures of complicated shape," *Journal of Optical Society Am.*, A11, No. 10, pp. 2664-2674, October 1994.
4. D. Mas, J. Garcia, C. Ferreira, L M. Bernardo, and F. Marinho, "Fast algorithm for free-space diffraction patterns calculation," *Optical Communication*, 164, pp. 233-245, June 1999.
5. S.-C. Pei, M.-H. Yeh, and C.-C. Tseng, "Discrete fractional Fourier transform based on orthogonal projections," *IEEE Transactions on Signal Processing*, Vol. 47, No. 5, pp. 1335-1348, May 1999.
6. H. M. Ozaktas, Z. Zalevsky and M. A. Kutay, *The Fractional Fourier Transform With Applications In Optics And Signal Processing*, Chichester, U.K: Wiley, 2001.
7. J. H. McClellan and T. W. Parks, "Eigenvalue and eigenvector decomposition of the Discrete Fourier Transform," *IEEE Transactions on Audio and Electroacoustics*, Vol. AU-20, No. 1, pp. 66-75, March 1972.
8. B. Santhanam and J.H. McClellan, "The discrete rotational Fourier transform," *IEEE Transactions on Signal Processing*, Vol. SP-44, No. 4, pp. 994-998, April 1996.
9. S.-C. Pei, C.-C. Tseng and M.-H. Yeh, "A new discrete fractional Fourier transform based on constrained eigendecomposition of DFT matrix by Lagrange multiplier method," *IEEE Transactions on Circuits and Systems, Part II: Analog and Digital Signal Processing*, Vol. 46, No. 9, pp. 1240-1245, September 1999.

10. B.W. Dickinson and K. Steiglitz, "Eigenvectors and functions of the discrete Fourier transform," *IEEE Transactions on Acoustics, Speech and Signal Processing*, vol. ASSP-30, pp. 25-31, February 1982.
11. Ç. Candan, M.A. Kutay and H.M. Ozaktas, "The discrete fractional Fourier transform," *IEEE Transactions on Signal Processing*, vol. SP-48, pp. 1329-1337, May 2000.
12. M.T. Hanna, N.P.A. Seif and W.A. Ahmed, "Hermite-Gaussian-Like Eigenvectors of the Discrete Fourier Transform Matrix Based on the Singular-Valued Decomposition of Its Orthogonal Projection Matrices," *IEEE Transactions on Circuits and Systems, Part I: Regular papers*, Vol. 51, No. 11, pp. 2245-2254, November 2004.
13. M.T. Hanna, N.P.A. Seif and W.A. Ahmed, "Hermite-Gaussian-Like Eigenvectors of the Discrete Fourier Transform Matrix Based on the Direct Utilization of the Orthogonal Projection Matrices on its Eigenspaces," *IEEE Transactions on Signal processing*, Vol. 54, No. 7, pp. 2815-2819, July 2006.
14. Ç. Candan, "On higher order approximations for Hermite-Gaussian functions and discrete fractional Fourier transforms," *IEEE Signal Processing Letters*, vol. 14, no. 10, pp. 699-702, October 2007.
15. S.-C. Pei, W.L. Hsue and J.J. Ding, "DFT-commuting matrix with arbitrary or infinite order second derivative approximation," *IEEE Transactions on Signal Processing*, vol. 57, no. 1, pp. 390-394, January 2009.
16. A. Serbes and L. Durak-Ata, "Efficient computation of DFT commuting matrices by a closed-form infinite order approximation to the second differentiation matrix," *Signal Processing*, vol. 91, no. 3, pp. 582-589, 2011.
17. H.M. Ozaktas, O. Arikan, M.A. Kutay and G. Bozdağı, "Digital Computation of the Fractional Fourier Transform," *IEEE Transactions on Signal Processing*, Vol. 44, No. 9, pp. 2141-2150, September 1996.
18. Alan V. Oppenheim, and Ronald W. Schaffer, *Discrete-Time Signal Processing*, Englewood Cliffs, N. J.: Prentice-Hall, 1989.
19. W. Gander and W. Gautschi, "Adaptive Quadrature-Revised," *Bit Numerical Mathematics Journal D*, Vol. 40, No. 1, pp. 84-101, March 2000.
20. M. Zamboni-Rached, E. Recami and H.E.Hernández-Figueroa, "New localized superluminal solutions to the wave equations with finite total energies and arbitrary frequencies," *European Physical Journal D*, Vol. 21, pp.217-228, 2002.
21. T. Alieva and M. J. Bastiaans, "Mode analysis in optics through fractional transforms," *Opt. Lett.*, **24**, pp. 1206-1208, 1999.

22. Hong-Yi Fan and Hai-Liang Lu, "Eigenmodes of fractional Hankel transform derived by the entangled-state method," *Opt. Lett.*, **28**, pp. 680-682, May 2003.
23. Li Yu, Yingyang Lu, Xiaoming Zeng, Meichun Huang, Mouzhi Chen, Wenda Huang, and Zizhong Zhu, "Deriving the integral representation of a fractional Hankel transform from a fractional Fourier transform," *Opt. Lett.*, **23**, pp. 1158-1160, 1998.
24. Zhangrong Mei and Daomu Zhao, "Propagation of Laguerre–Gaussian and elegant Laguerre–Gaussian beams in apertured fractional Hankel transform systems," *J. Opt. Soc. Am. A* **21**, pp. 2375-2381, 2004.

Table (1) The execution time of the **RALQ method** and DFRFT method for evaluating the 1-D Fresnel Integral ($\lambda = 0.025L$).

Method	Execution Time hh:mm:ss
DFRFT ($N = 70$).	00:00:00.07
DFRFT ($N = 500$).	00:00:04
RALQ method	00:01:26.08

Table (2) The execution time of the 2-D **RALQ method** and DFRFT method for evaluating the 2-D Fresnel Integral ($\lambda = 0.025L$).

Method	Execution Time hh:mm:ss
DFRFT ($N = 70$)	00:00:20
RALQ method.	30:01:10

Table (3) The execution time of the **RALQ method** and DFRFT method for evaluating the pulse illumination pattern ($\Delta x = 0.1$ and $c \Delta t = 0.01$).

Method	Execution Time hh:mm:ss
DFRFT ($N = 100$).	00:00:50
RALQ method	04:31:20

FIGURE CAPTIONS

Figure 1. (Color Online) (a) The real and (b) imaginary parts of the diffraction pattern at $d = 2.5L$. The solid lines are obtained by evaluating Fresnel Integral using the **RALQ** method. The dots are points calculated using DFRFT with $N = 500$. The width of the slit is $2L = 4$ and $\lambda = 0.025L$.

Figure 2. (Color Online) (a) The real and (b) imaginary parts of the diffraction pattern at $d = 2.5L$. The solid lines are obtained by evaluating Fresnel Integral using the **RALQ** method. The dots are points calculated using DFRFT with $N = 70$. The width of the slit is $2L = 4$ and $\lambda = 0.025L$.

Figure 3. (Color Online) (a) The real and (b) imaginary parts of the diffraction pattern at $d = L$. The solid lines are obtained by evaluating Fresnel Integral using the **RALQ** method. The dots are points calculated using DFRFT with $N = 500$. The width of the slit is $2L = 4$ and $\lambda = 0.001L$.

Figure 4. (Color Online) (a) The real and (b) imaginary parts of the diffraction pattern at $d = L$. The solid lines are obtained by evaluating Fresnel Integral using the **RALQ** method. The dots are points calculated using DFRFT with $N = 70$. The width of the slit is $2L = 4$ and $\lambda = 0.001L$.

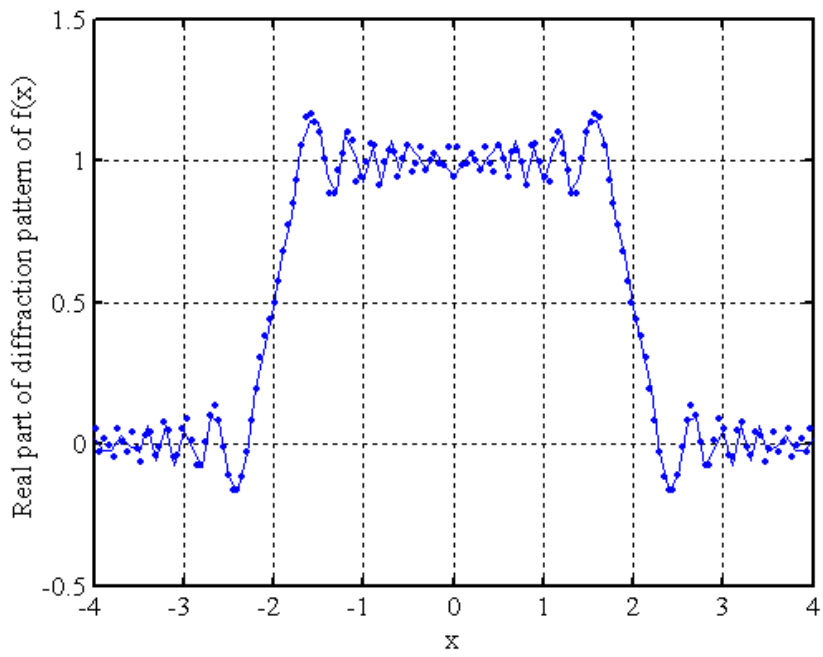
Figure 5. (Color Online) The real part of the amplitude distribution of diffraction pattern using (a) the **RALQ** and (b) the DFRFT method ($N = 70$). The distance is $d = 0.25 L_1$, $\lambda = 0.025L_1$, and the dimension of the aperture $2L_1 \times 2L_2 = 4 \times 4$.

Figure 6. (Color Online) The real part of the amplitude distribution of the diffraction pattern using (a) the **RALQ method** and (b) the DFRFT method ($N = 70$). The distance is $d = 0.25 L_1$, $\lambda = 0.00025L_1$, and the dimension of the aperture $2L_1 \times 2L_2 = 4 \times 4$.

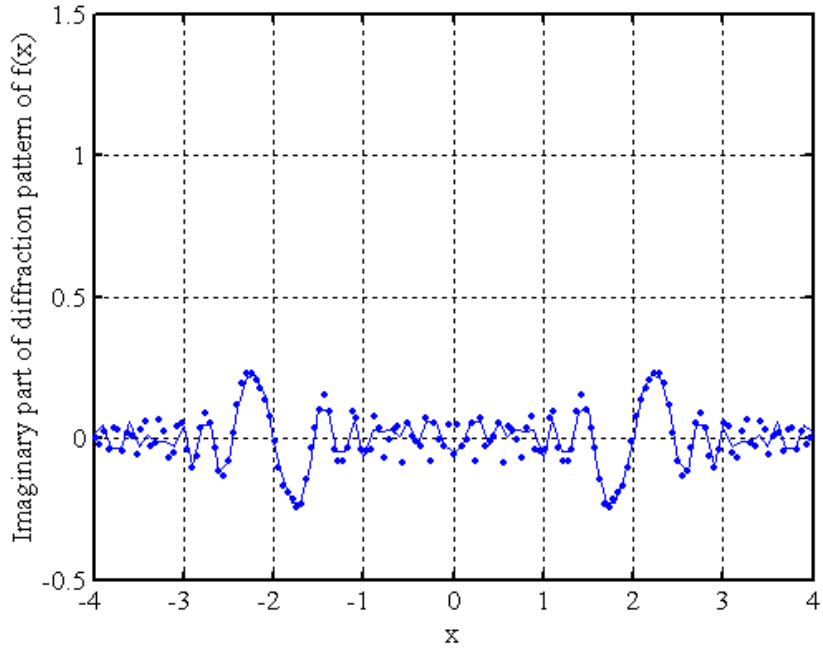
Figure 7. (Color Online) The spectrum of the pulsed field at the aperture ($b(k)$ of Eq. (41))

Figure 8. (Color Online) The field of a pulse radiated from a slit and evaluated at $d = 0.5L$ using (a) the **RALQ method** and (b) the DFRFT.

Figure 9. (Color Online) The profile of the radiated pulse at $x = L$, using the **RALQ method** (solid line) and DFRFT method (dots).

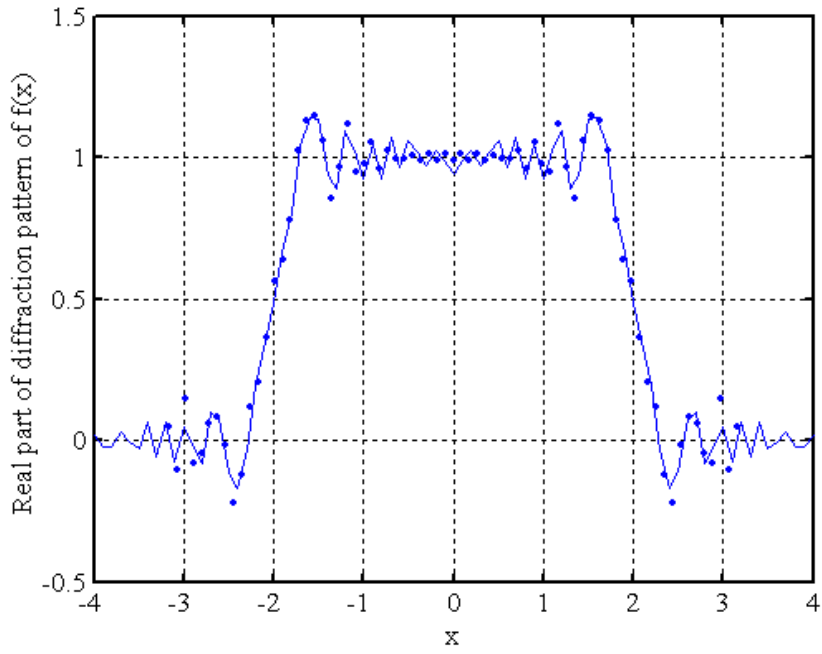


(a)

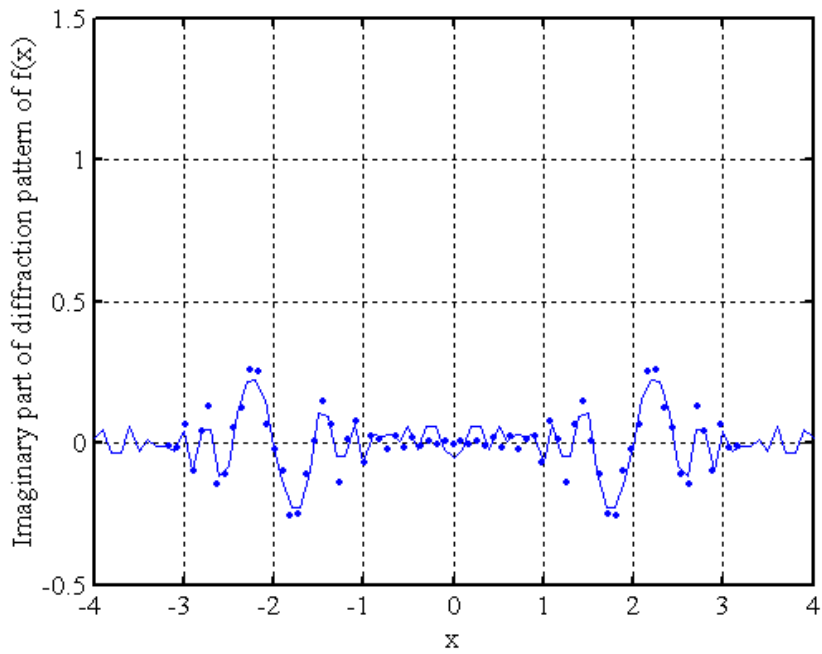


(b)

Figure (1)

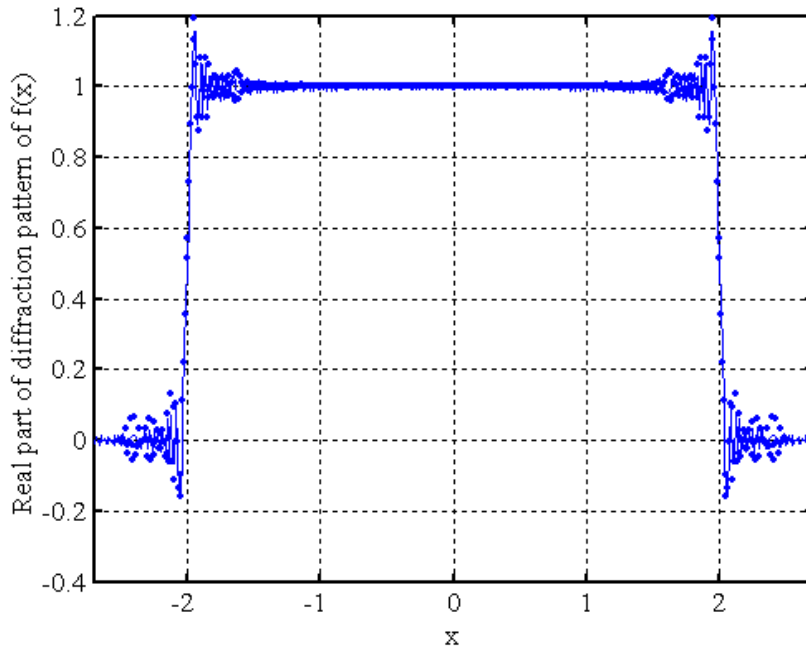


(a)

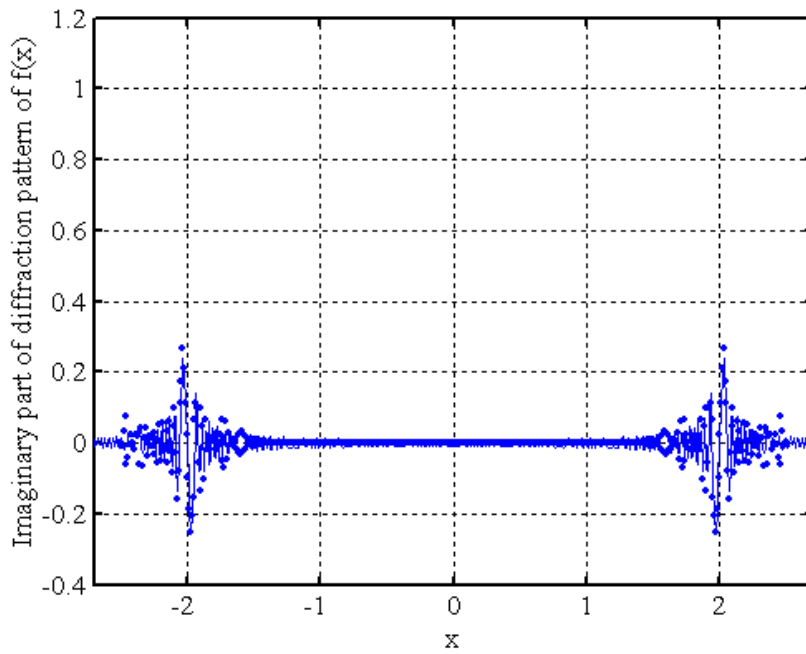


(b)

Figure (2)

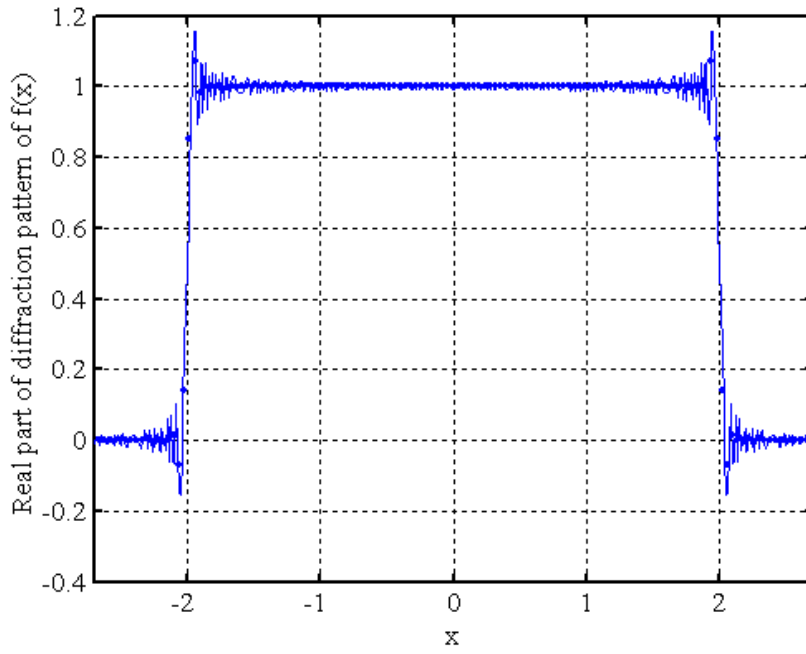


(a)

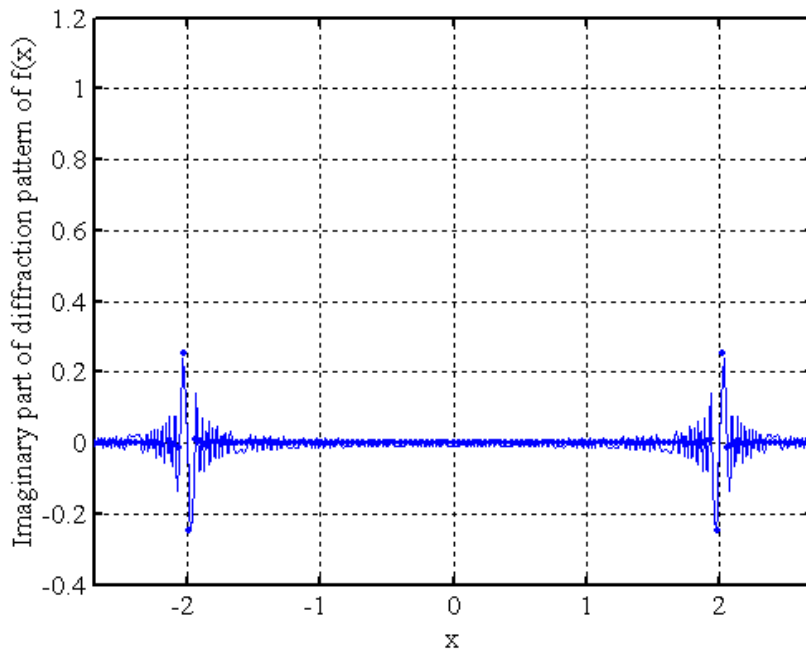


(b)

Figure (3)

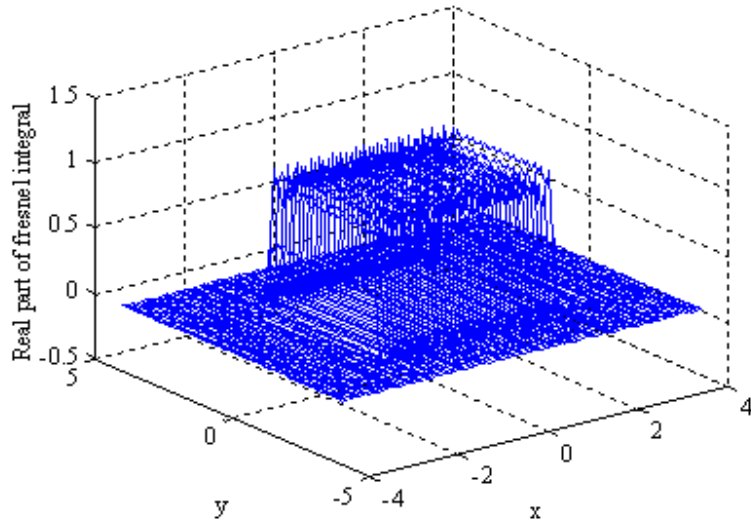


(a)

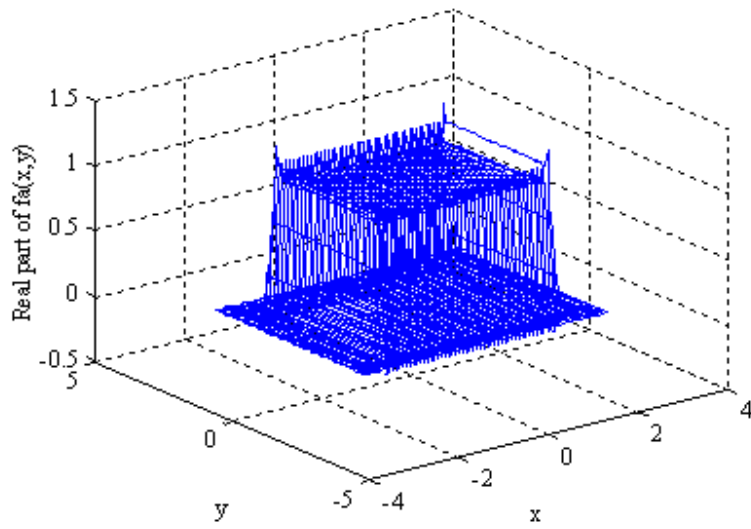


(b)

Figure (4)

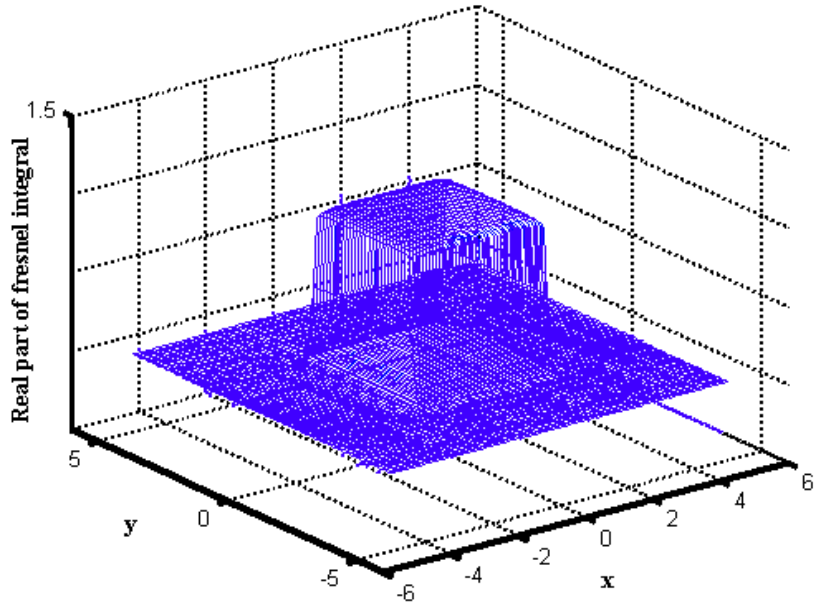


(a)

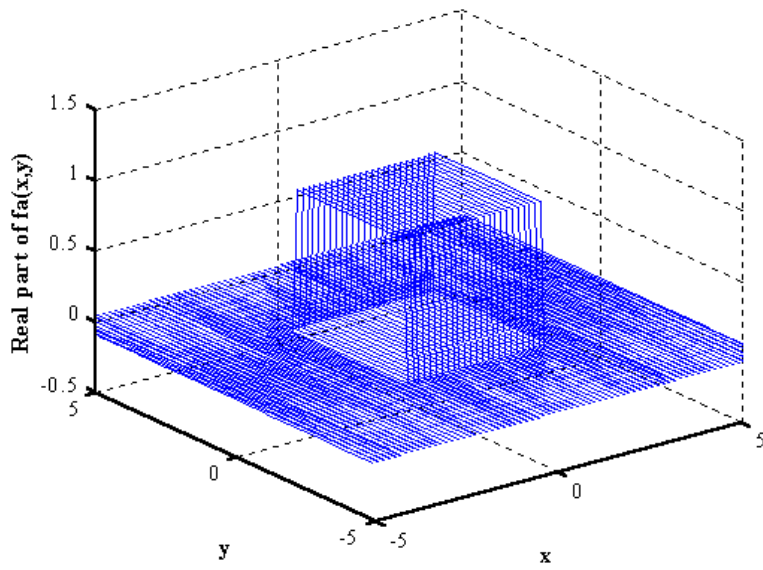


(b)

Figure (5)



(a)



(b)

Figure (6)

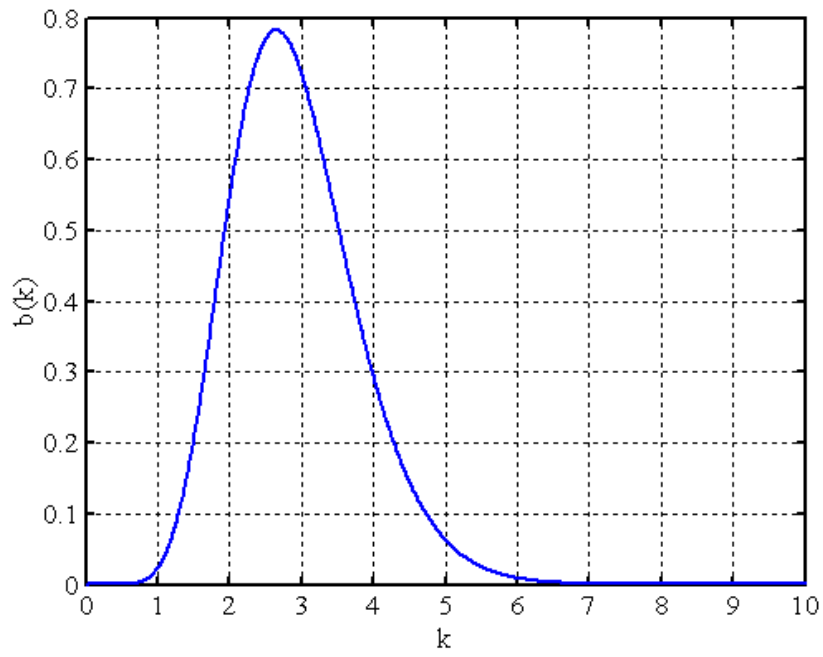
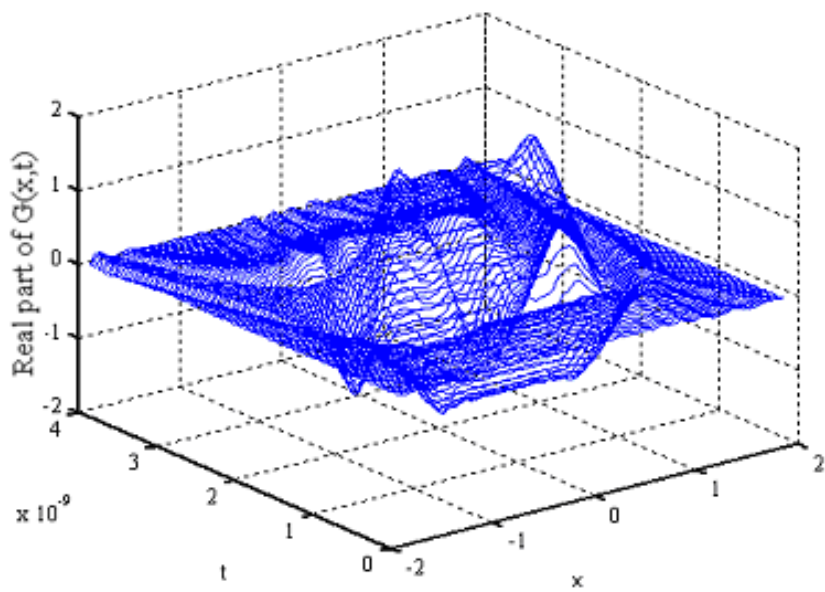
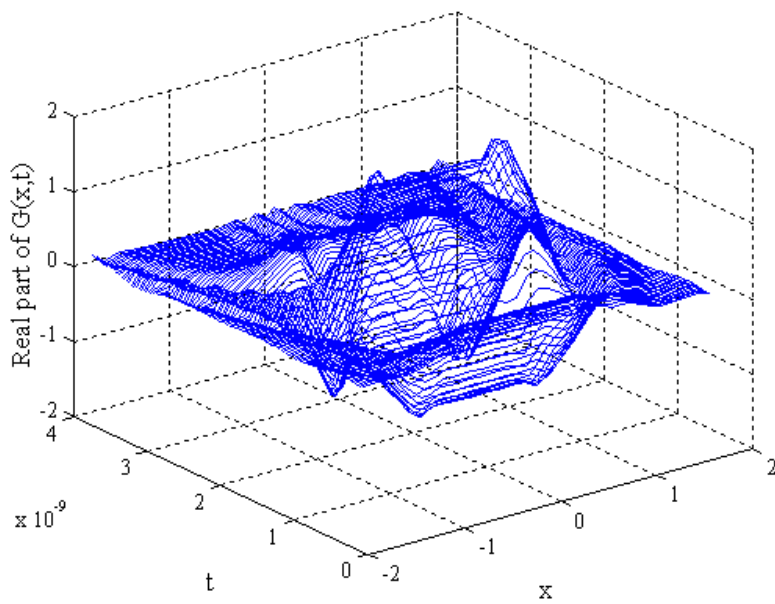


Figure (7)



(a)



(b)

Figure (8)

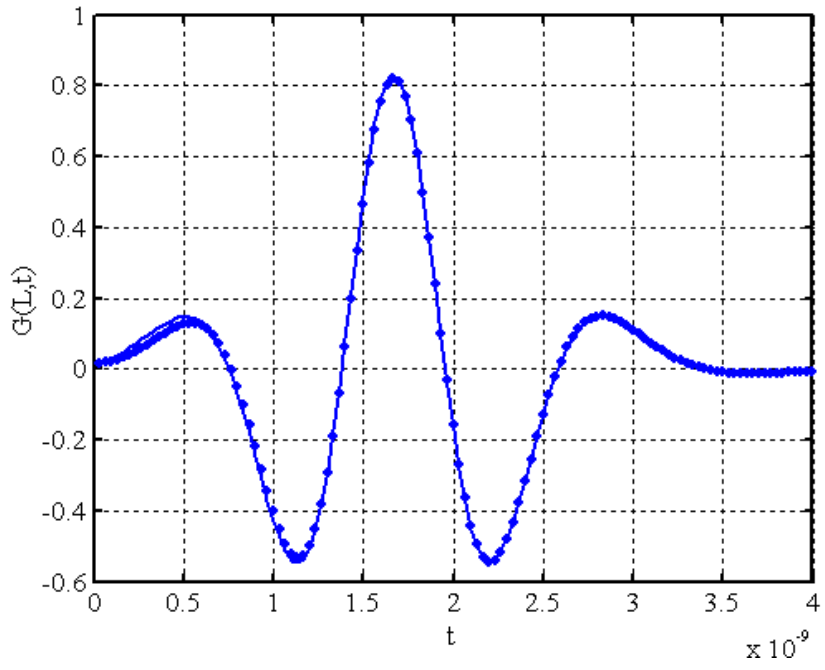


Figure (9)